Hindawi Publishing Corporation
EURASIP Journal on Wireless Communications and Networking
Volume 2009, Article ID 715403, 15 pages
doi:10.1155/2009/715403

Research Article

Polarimetric Kronecker Separability of Site-Specific Double-Directional Channel in an Urban Macrocellular Environment

Kriangsak Sivasondhivat,[1] Jun-Ichi Takada,[2] Ichirou Ida,[3] and Yasuyuki Oishi[3]

[1] *Agilent Technologies Japan, Ltd., Kobe-shi, Hyogo, 651-2241, Japan*
[2] *Department of International Development Engineering (IDE), Graduate School of Science and Technology, Tokyo Institute of Technology, Tokyo 152-8550, Japan*
[3] *Fujitsu, Ltd., Fujitsu Laboratory, Yokosuka-shi, 239-0847, Japan*

Correspondence should be addressed to Kriangsak Sivasondhivat, sivasondhivat.kriangsak@gmail.com

Received 2 August 2008; Revised 22 November 2008; Accepted 7 January 2009

Recommended by Persefoni Kyritsi

This paper focuses on the modeling of a double-directional power spectrum density (PSD) between the base station (BS) and mobile station (MS) based on the site-specific measurements in an urban macrocell in Tokyo. First, the authors investigate the Kronecker separability of the joint polarimetric angular PSD between the BS and MS by using the ergodic mutual information. The general form of the sum of channel polarization pair-wise Kronecker product approximation is proposed to be used to model the joint polarimetric angular PSD between the BS and MS. Finally, the double-directional PSD channel model is proposed and verified by comparing the cumulative distribution functions (CDFs) of the measured and modeled ergodic mutual information.

1. Introduction

It has been shown that the use of multiple antennas at a base station (BS) and a mobile station (MS), called as multiple input multiple output (MIMO) system, can promisingly increase the data rate [1]. However, low correlation between antennas is required in MIMO systems, in order to ensure the data rate improvement [2]. This implies the need of large antenna spacing, resulting in the size increase of the system. As a candidate scheme to achieve the low correlation in compact MIMO systems, the application of multiple polarizations to MIMO systems has been increasingly investigated [3–6].

To evaluate and compare MIMO systems with multiple polarizations, a channel model having the polarimetric information in addition to azimuth and elevation angles at the BS and MS is obviously needed [7, 8]. Recently, for outdoor environments, standard channel models having such information for polarimetric MIMO systems have been defined in the spatial channel model (SCM), which was presented in the 3rd Generation Partnership Project (3GPP) standard body [9], and in the European co-operation in the field of scientific and technical research (COST) actions 273 [10]. The further analytical extension of the SCM to the 3D case has been recently done by Shafi et al., in [11].

Since the degree of depolarization of a propagation channel directly affects the performance of the MIMO systems with multipolarizations [12], a channel model must accurately reproduce the polarization behavior of the channel. However, due to the lack of reliable tools to reproduce polarization mechanisms, the derivation of the polarimetric channel model from measurements is still of great significance [13–15].

Moreover, it is also important that a channel model is applicable to any arbitrary array antennas under development, the channel model must thus be independent of the measurement antennas, which is known as the double-directional channel model [16, 17]. It should be noted that double-directional channel models aim to present the physical channel propagation alone by describing the parameters

of multipaths. They are different from conventional channel models, which mainly aim to present the statistics of a transfer function between the BS and MS and thus the effect of measurement antennas are included. Independent and identically distributed (i.i.d.) Rayleigh and correlation matrices-based MIMO channel models such as Kronecker [2, 18] and Weichselberger et al., [19] MIMO channel models are good examples of conventional channel models.

In [20], the authors have proposed an angular-delay power spectrum density (PSD) channel model at the MS based on a 3D double-directional measurements in a residential urban area in Tokyo. The PSD channel model was shown to be able to predict the eigenvalue distributions of a diversity system assumed for the MS. In this paper, the authors focus on a site-specific double-directional PSD channel model by extending the directional PSD channel model at the MS.

To do so, the following contributions are done.

(i) First, to motivate the study of channel modeling for multiple polarized MIMO systems, the polarization characteristics of the measured channel are investigated. The benefit of exploiting a polarization diversity is next shown by using the measurement antennas.

(ii) Then, the separability of the joint polarimetric angular PSD between the BS and MS of the measured propagation channel, which is a necessary assumption for the angular-delay PSD channel model in [20] when extended to the double-directional PSD channel model, is investigated. This is done by investigating the Kronecker separability of a joint correlation matrix of reference polarized antennas at the BS and MS.

The standard antenna configurations of a 3GPP LTE channel model are used as reference in the evaluations of the Kronecker separability, which are based on the ergodic mutual information.

(iii) It should be noted that in the conventional Kronecker product [2, 18], when single polarized antennas are used at the BS and the MS, the validity of the Kronecker separability of the joint correlation matrix shows how well the joint angular PSD between the BS and MS can be modeled as the product of the marginal angular PSDs [21].

However, for multiple polarized MIMO systems, the conventional Kronecker product is not suitable to be used for evaluating the separability of the joint angular PSD since the propagation channel polarizations are mixed with the antenna polarizations. Moreover, the angular-delay PSD channel model at the MS in [20] was proposed for each channel polarization-pair, so the Kronecker separability of the joint correlation matrix must be investigated for each channel polarization-pair as well.

The authors propose a general form of the sum of channel polarization pair-wise Kronecker product approximation, which is shortly called "sum of Kronecker products" herewith, to investigate the separability of the joint polarimetric angular PSD. By using the proposed sum of Kronecker products, the error of the assumption that the joint correlation matrix can be separated for each polarization-pair is investigated. Also, its validity is compared with the following Kronecker product approximations:

(a) conventional Kronecker product,

(b) 3GPP long-term evolution (3GPP LTE) Kronecker product [22].

(iv) Next, the polarimetric angular PSD models at the BS are studied and their best-fit parameters are derived. Then, by using the proposed sum of Kronecker products, a double-directional PSD channel model is presented. Finally, this double-directional PSD channel model is evaluated by comparing the ergodic mutual information of 3GPP LTE system scenario.

It should be noted that even though the validation of Kronecker separability based on the proposed sum of Kronecker products is done by using the standard antenna configurations of a 3GPP LTE channel model, the term "double-directional PSD channel model" is used here for the presented PSD channel model due to the fact that extracted channel parameters are independent of the measurement antennas since the beam patterns of the measurement antennas are taken into account in the multipath parameters extraction [20].

This paper is organized as follows. Section 2 explains the measurement system, measurement environment, and the extraction of multipaths parameters. In Section 3, the mathematical expression of a polarimetric MIMO channel matrix is first given. Following this, the polarization characteristics of the measured channel are investigated and then the effect of exploiting a polarization diversity is studied. In Section 4, the concepts of different Kronecker product approximations, that is, conventional Kronecker product, 3GPP LTE Kronecker product, and sum of Kronecker products proposed by the authors are explained. The comparison among Kronecker product approximations is done in Section 5. Based on the validity of sum of Kronecker products shown in Section 5, the double directional PSD channel model is presented in Section 6. Section 7 presents the result of the evaluation of the double directional PSD channel model. Finally, the conclusion is given in Section 8.

2. Measurement and Channel Parameters Extraction

The double-directional measurements were carried out in a residential urban area in Minami-Senzoku, Ota-ku, Tokyo. The measurement site consists of 4 streets, which were divided into the measurement segments of about 10 m. The MS was moved continuously to collect consecutive snapshots. The BS antenna used was a 2×4 polarimetric uniform rectangular antenna array of dual-polarized patch antenna elements. At the MS side, a 2×24 polarimetric circular

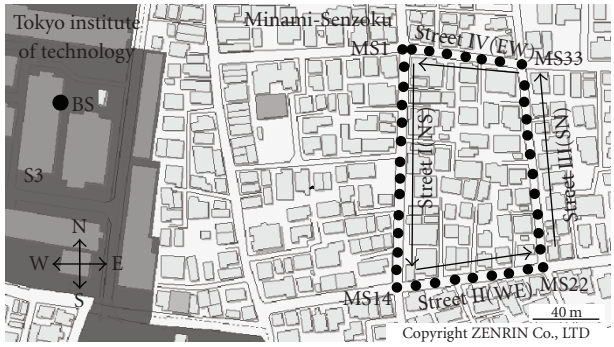

Figure 1: Measurement site map.

Table 1: Measurement parameters.

Center frequency	4.5 GHz
Bandwidth	120 MHz
Excess delay window	3.2 μs
Transmitting power	10 W
BS antenna height	30 m
MS antenna height	1.65 m
Total measurement length	380 m
Total measurement snapshots	872
Distance to the BS	186 m –276 m

antenna array was used. The measurement was explained in detail in [20]. Figure 1 shows the measurement map. Note that the arrows in the figure show the moving direction of the MS. The important parameters are summarized in Table 1.

By using a multidimensional gradient-based maximum-likelihood estimator [23], multipath parameters were extracted. A path is modeled as an optical ray with the azimuth at BS (ABS), elevation at BS (EBS), azimuth at MS (AMS), elevation at MS (EMS), delay, and a matrix of polarimetric complex path weights, respectively. For the kth multipath, it is modeled by

$$\begin{bmatrix} \gamma_{\mathrm{VV},k} & \gamma_{\mathrm{VH},k} \\ \gamma_{\mathrm{HV},k} & \gamma_{\mathrm{HH},k} \end{bmatrix} \delta(\phi^{\mathrm{BS}} - \phi_k^{\mathrm{BS}})\delta(\vartheta^{\mathrm{BS}} - \vartheta_k^{\mathrm{BS}})\delta(\phi^{\mathrm{MS}} - \phi_k^{\mathrm{MS}}) \times \delta(\vartheta^{\mathrm{MS}} - \vartheta_k^{\mathrm{MS}})\delta(\tau - \tau_k), \tag{1}$$

where $\gamma_{\mathrm{VV},k}$, $\gamma_{\mathrm{HV},k}$, $\gamma_{\mathrm{VH},k}$, and $\gamma_{\mathrm{HH},k}$ are the polarimetric complex path weights. The first and the second subscripts show polarizations at the MS and BS, respectively. In this paper, vertical and horizontal polarizations are defined as ϑ and ϕ components of electric field. It is assumed that the vertically placed infinitesimal electric and magnetic dipoles as the reference vertically and horizontally polarized antennas. This corresponds to Ludwig's Definition 2 of the polarization [24].

The quantities ϕ_k^{BS}, $\vartheta_k^{\mathrm{BS}}$, ϕ_k^{MS}, $\vartheta_k^{\mathrm{MS}}$, and τ_k denote the ABS, EBS, AMS, EMS, and delay, respectively. The definitions of the angle parameters at the BS and MS are depicted in Figure 2. It should be noted that the extracted polarimetric complex path weights were made independent of the measurement antennas by incorporating the measured beam patterns of the BS and MS antennas in the multipath parameters estimator.

The measurement site is mostly characterized by nonline-of-sight (NLOS) conditions. For some line-of-sight (LOS) measurement snapshots, since their LOS paths are deterministic, they are removed from the extracted multipaths, so that the considered channel becomes zero-mean complex circularly symmetric Rayleigh in order to model the NLOS component.

3. Polarimetric MIMO Channel Matrix, Polarization Characteristics, and Effect of Polarization Diversity

3.1. Polarimetric MIMO Channel Matrix. For wideband MIMO systems having N_{BS} and N_{MS} antennas at the BS and MS, respectively, where $n_{\mathrm{MS}} = 1, \ldots, N_{\mathrm{MS}}$ and $n_{\mathrm{BS}} = 1, \ldots, N_{\mathrm{BS}}$, the $(n_{\mathrm{MS}}, n_{\mathrm{BS}})$ element of a MIMO channel matrix at the frequency f, $\mathbf{H}(f)$, can be expressed as a sum of channel responses of all polarization-pairs, that is,

$$[\mathbf{H}(f)]_{n_{\mathrm{MS}}n_{\mathrm{BS}}} = \sum_{\alpha,\beta=\{\mathrm{V,H}\}} [\mathbf{H}_{\beta\alpha}(f)]_{n_{\mathrm{MS}}n_{\mathrm{BS}}}, \tag{2}$$

where $[\mathbf{H}_{\beta\alpha}(f)]_{n_{\mathrm{MS}}n_{\mathrm{BS}}}$ denotes the $(n_{\mathrm{MS}}, n_{\mathrm{BS}})$ element of single polarization $\mathbf{H}(f)$ of a $\{\beta\alpha\}$ polarization-pair. Note that $[\mathbf{H}(f)]_{n_{\mathrm{MS}}n_{\mathrm{BS}}}$ and $[\mathbf{H}_{\beta\alpha}(f)]_{n_{\mathrm{MS}}n_{\mathrm{BS}}}$ are defined in the downlink direction. Accordingly, β and α show the channel polarization at the MS and BS, respectively.

By using the extracted multipaths in Section 2, $[\mathbf{H}_{\beta\alpha}(f)]_{n_{\mathrm{MS}}n_{\mathrm{BS}}}$ can be expressed as the superposition of all multipaths between the BS and MS as follows:

$$[\mathbf{H}_{\beta\alpha}(f)]_{n_{\mathrm{MS}}n_{\mathrm{BS}}} = \sum_{k=1}^{K} \gamma_{\beta\alpha,k}\, g_{\beta}^{n_{\mathrm{MS}}}(\phi_k^{\mathrm{MS}}, \vartheta_k^{\mathrm{MS}}) g_{\alpha}^{n_{\mathrm{BS}}}(\phi_k^{\mathrm{BS}}, \vartheta_k^{\mathrm{BS}}) \times \exp\left(j[\langle \mathbf{k}_k^{\mathrm{MS}}(f), \vec{r}_{n_{\mathrm{MS}}}\rangle + \langle \mathbf{k}_k^{\mathrm{BS}}(f), \vec{r}_{n_{\mathrm{BS}}}\rangle] - j2\pi f \acute{\tau}_k + j\nu_k^{\beta\alpha}\right), \tag{3}$$

where K = the number of extracted multipaths, $g_{\alpha}^{n_{\mathrm{BS}}}(\cdot)$ = the complex amplitude gain of α component, electric field of the n_{BS}th element, $g_{\beta}^{n_{\mathrm{MS}}}(\cdot)$ = the complex amplitude gain of β component, electric field of the n_{MS}th element, $\mathbf{k}_k^{\mathrm{BS}}(\cdot)$ = the wave vector at the BS, $\mathbf{k}_k^{\mathrm{MS}}(\cdot)$ = the wave vector at the MS, $\vec{r}_{n_{\mathrm{BS}}}$ = the position vector of the n_{BS}th element, $\vec{r}_{n_{\mathrm{MS}}}$ = the position vector of the n_{MS}th element, $\langle\cdot,\cdot\rangle$ = the inner product of two vectors, $\acute{\tau}_k$ = the excess delay, that is, $\tau_k - \tau_0$, τ_0 = the delay of the first arriving multipath at a snapshot, and $\nu_k^{\beta\alpha}$ = a uniformly distributed random phase from 0 to 2π [25, 26].

In general, the vector amplitude gain of an antenna element at either the BS or MS can be expressed as

$$g_{\mathrm{H}}(\phi,\vartheta)\mathbf{u}_{\mathrm{H}}(\phi,\vartheta) + g_{\mathrm{V}}(\phi,\vartheta)\mathbf{u}_{\mathrm{V}}(\phi,\vartheta), \tag{4}$$

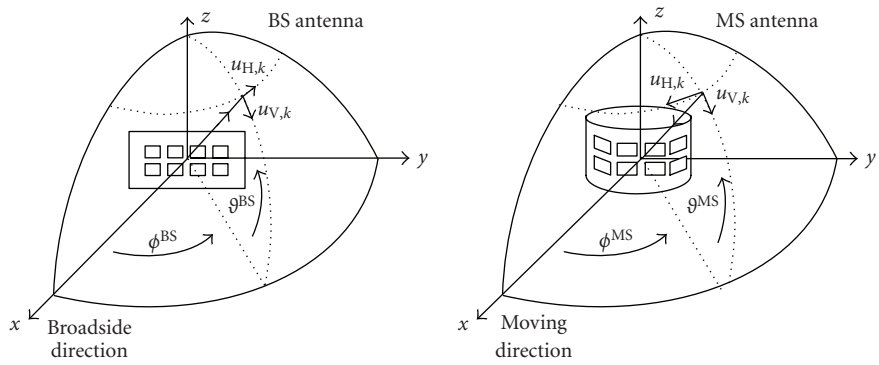

Figure 2: Coordinate systems at the BS and MS.

where $\mathbf{u}_H(\phi, \vartheta)$ and $\mathbf{u}_V(\phi, \vartheta)$ are the H and V polarization vectors in the direction (ϕ, ϑ), respectively. For the kth multipath, $\mathbf{u}_{\alpha,k}(\phi_k^{BS}, \vartheta_k^{BS})$ and $\mathbf{u}_{\beta,k}(\phi_k^{MS}, \vartheta_k^{MS})$ are depicted in Figure 2. It should be noted that $[\mathbf{H}_{\beta\alpha}(f)]_{n_{MS}n_{BS}}$ is normalized with respect to the delay of the first arriving multipath.

Moreover, when synthesizing $\mathbf{H}_{\beta\alpha}(f)$, their realizations are independently generated based on the Monte Carlo simulations of $\nu_k^{\beta\alpha}$. Since in this paper the authors focus on the Kronecker separability of the measured channel, and that the $\mathbf{H}(f)$'s have the same spatial correlation characteristic, $\mathbf{H}(f)$'s can be thus considered as different realizations of the random MIMO channel matrices. Accordingly, $\mathbf{H}(f)$ is simply expressed as $\mathbf{H}$.

3.2. Polarization Characteristics of the Measured Channel. Herein, the term cross-polarization ratio (XPR) is used for the depolarization of each extracted path and can be obtained at both the BS and MS as follows:

$$\begin{aligned}
\mathrm{XPR}_V^{BS}\,[\mathrm{dB}] &= 10\log_{10}\left(\frac{|\gamma_{VV}|^2}{|\gamma_{VH}|^2}\right),\\
\mathrm{XPR}_H^{BS}\,[\mathrm{dB}] &= 10\log_{10}\left(\frac{|\gamma_{HH}|^2}{|\gamma_{HV}|^2}\right),\\
\mathrm{XPR}_V^{MS}\,[\mathrm{dB}] &= 10\log_{10}\left(\frac{|\gamma_{VV}|^2}{|\gamma_{HV}|^2}\right),\\
\mathrm{XPR}_H^{MS}\,[\mathrm{dB}] &= 10\log_{10}\left(\frac{|\gamma_{HH}|^2}{|\gamma_{VH}|^2}\right).
\end{aligned} \tag{5}$$

For a certain path, XPR shows how much the V polarization component changes to the H polarization component, or vice versa. Due to the antenna deembedding, XPR is purely from a propagation channel and does not change with a measurement antenna. It should be noted that when the effects of measurement antennas are also included, the term cross-polarization discrimination (XPD) is often used instead [27].

Table 2: XPRs and CPR.

	Mean [dB] (STD [dB])			
	street I	street II	street III	street IV
XPR_V^{BS}	10.2 (10.6)	6.9 (9.9)	9.6 (10.6)	10.4 (8.8)
XPR_H^{BS}	9.2 (9.0)	6.9 (8.2)	9.1 (9.3)	10.3 (8.5)
XPR_V^{MS}	10.7 (9.2)	8.3 (8.9)	10.8 (9.3)	10.8 (8.7)
XPR_H^{MS}	8.7 (9.4)	5.5 (8.7)	7.9 (9.5)	9.9 (8.8)
CPR	1.5 (8.6)	1.4 (8.7)	1.7 (8.9)	0.5 (7.6)

In addition to XPRs, the copolarization ratio (CPR), which is the power ratio of covertical polarization γ_{VV} to cohorizontal polarization γ_{HH},

$$\mathrm{CPR}\,[\mathrm{dB}] = 10\log_{10}\left(\frac{|\gamma_{VV}|^2}{|\gamma_{HH}|^2}\right) \tag{6}$$

is also necessary to describe the polarization characteristics of a path.

Figure 3 shows the cumulative distribution functions (CDFs) of XPRs and CPR at the BS and MS for all measurement streets. In the normal probability plot of CDFs, if data comes from a normal distribution, the plot will appear linear. Accordingly, the XPRs and CPR can be assumed to be a log-normal distribution. Table 2 shows means and standard deviations (STDs) of XPRs and CPR. As shown in the table, the means of XPRs at the BS and MS have no big difference. Lowest XPRs are found in street II (WE), which is completely NLOS, and thus the more number of scatterings is expected [20]. While, some obstructed LOS (OLOS) by rooftops in the south side of street IV (EW) cause the highest XPRs among all measurement streets.

On the other hand, the mean values of CPRs, which indicate the gainimbalance between V and H transmitting polarizations, are found to be 1.5, 1.4, 1.7, and 0.5 dB for street I (NS) to street IV (EW), respectively. Their positive values suggest that H polarization transmission have on average bigger attenuation compared to that of V polarization. In other words, the propagation in outdoor macrocellular is in favor of vertical transmission [28].

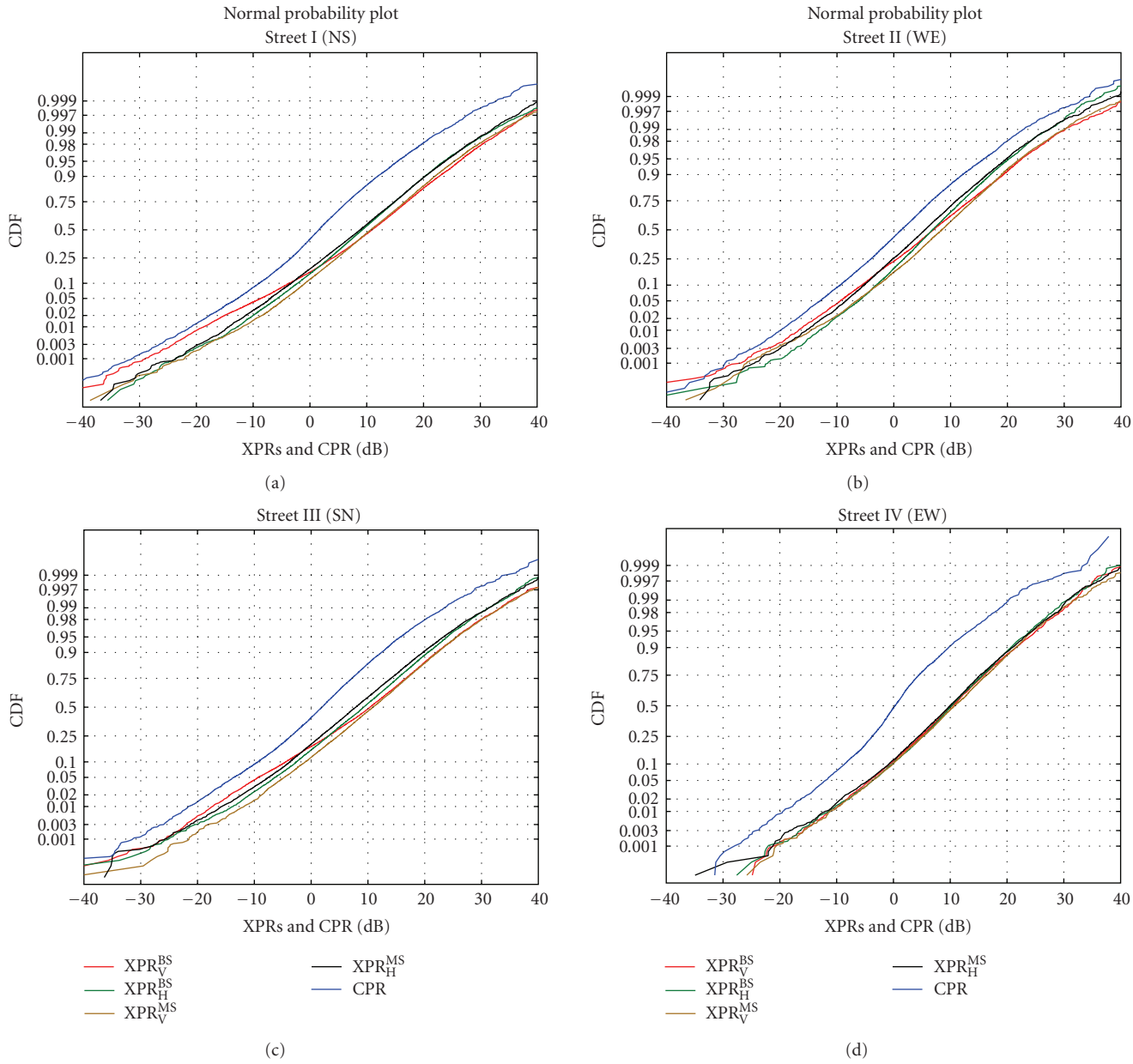

Figure 3: XPRs and CPR.

3.3. Effect of Polarization Diversity. To evaluate the contributions of polarizations, the mutual ergodic information, which is an important criterion from the viewpoint of maximum achievable data rate, of a multiple polarized MIMO system is compared with that of a single polarized MIMO system. 4×4 multiple polarized MIMO antennas are selected from the BS and MS measurement antenna arrays as shown in Figure 4. For a single polarized MIMO system, vertically polarized antenna elements of no. 1, 3, 5, and 7 at both ends are selected. While, the vertically and horizontally polarized antenna elements of no. 2, 3, 6, and 7 at the BS and 2, 3, 5, and 8 at the MS are selected for a multiple polarized MIMO system.

For each measurement snapshot, the authors synthesize measurement-based random MIMO channel matrices, $\mathbf{H}$, according to (2) by Monte Carlo simulations. Each channel realization is generated by the random phase method using (3). The number of the realizations, N_r, is set to 400. The number of the frequency bins, N_f, is set to 25 within a bandwidth of 120 MHz, resulting to a channel separation of 5 MHz at each frequency bin. To take into account the change of the antenna orientation during the movement of the MS, the N_a combinations of antenna array orientation are also considered for each measurement snapshot. N_a is set to 8 with the step of 45°.

In case that the total power is equally allocated to each BS antenna element and assuming that the channel state information is only known at the MS [1], the ergodic mutual information, $\mathcal{I}(n_a)$, of the n_ath MS orientation, where $n_a = 1, \ldots, N_a$, is given by

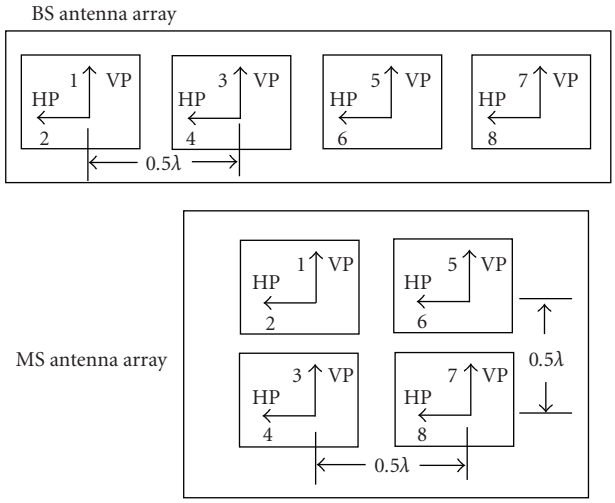

Figure 4: Selected BS and MS antenna arrays.

$$\mathcal{I}(n_a) = E\left[\log_2 \det\left(\mathbf{I}_{N_{\mathrm{MS}}} + \frac{\mathrm{SNR}}{N_{\mathrm{BS}}}\widetilde{\mathbf{H}}(n_a)\widetilde{\mathbf{H}}^H(n_a)\right)\right], \quad (7)$$

where $\mathbf{I}_{N_{\mathrm{MS}}}$ denotes the identity matrix of size N_{MS}, and SNR is the average signal-to-noise ratio at the MS. The expectation is approximated by the sample average of the $N_r \times N_f$ realizations of $\widetilde{\mathbf{H}}(n_a)$.

To appropriately evaluate the use of multiple polarizations, the normalized instantaneous MIMO channel matrices, $\widetilde{\mathbf{H}}^{(n_r,n_f)}(n_a)$s, where $n_r = 1,\ldots,N_r$ and $n_f = 1,\ldots,N_f$, of both single and multiple polarized MIMO systems are obtained with respect to the single polarized MIMO system. In other words, the SNR is defined for the single polarized MIMO system. Thus, for each instantaneous MIMO channel matrix, $\mathbf{H}^{(n_r,n_f)}(n_a)$, $\widetilde{\mathbf{H}}^{(n_r,n_f)}(n_a)$ is obtained as

$$\widetilde{\mathbf{H}}^{(n_r,n_f)}(n_a) = \frac{\mathbf{H}^{(n_r,n_f)}(n_a)}{\sqrt{(1/N_r N_f N_a N_{\mathrm{BS}} N_{\mathrm{MS}}) \sum_{n_r=1}^{N_r}\sum_{n_a=1}^{N_a}\sum_{n_f=1}^{N_f} \left\|\mathbf{H}_{\mathrm{single}}{}^{(n_r,n_f)}(n_a)\right\|_F^2}}, \quad (8)$$

where $\|\cdot\|_F$ is the Frobenius norm and $\mathbf{H}_{\mathrm{single}}{}^{(n_r,n_f)}(n_a)$ is the $\mathbf{H}^{(n_r,n_f)}(n_a)$ of the single polarized MIMO system.

$\mathbf{H}^{(n_r,n_f)}(n_a)$ is obtained by replacing ϕ_k^{MS} with $\{\phi_k^{\mathrm{MS}} - \phi^{\mathrm{MS}}(n_a)\}$ in (3), where $\phi^{\mathrm{MS}}(n_a) = 0^\circ, 45^\circ, \ldots, 315^\circ$ for $n_a = 1,\ldots,8$, respectively. It should be noted that the differences in received power fading among MS antenna orientations are also considered when calculating $\mathcal{I}(n_a)$ in addition to those realizations.

Figure 5 shows the ergodic mutual information of the single and multiple polarized MIMO systems at an SNR of 10 dB. It is clear from the figure that the polarization diversity promisingly increases the ergodic mutual information. When comparing the ergodic mutual information of both systems of each MS antenna orientation at all measurement snapshots, the average increases are 12%, 34%, 18%, and 26% for street I (NS) to street IV (EW), respectively.

4. Reference Scenario and Polarimetric Kronecker Product Approximations

In the previous section, the benefit of exploiting the polarization diversity in a MIMO system has been confirmed. Next, the validity of polarimetric Kronecker separability of the measured channel is investigated in this section. However, in principle, since the validity of polarimetric Kronecker separability depends not only on the characteristics of the channel, but also on the polarized antennas, some standard polarized antennas at the BS and MS have to be assumed in the investigation.

4.1. Reference Scenario. As reference antennas, the standard antenna configurations of the 3GPP LTE channel model are used (see Annex C of [22]). For the BS, an antenna configuration with 4 antenna elements, where 2 elements are dual at slants of $\pm 45^\circ$ is assumed. For the MS antenna, the authors assume *Laptop* scenario, which is shown in Figure 6. The results of the other MS scenarios, i.e., *handheld data* and *handheld talk*, are reported in [29]. Table 3 shows the details of the BS and MS antenna configurations and their parameter values with an azimuth power gain, $G(\phi)$, which is mathematically defined as follows: The vector amplitude gain of an antenna element at the BS and MS in (3) can thus be defined in terms of power gain and the element polarization vector, $\mathbf{p}$, i.e., $\sqrt{G(\cdot)}\mathbf{p}(\cdot)$. It should be noted that $G(\phi)$, which is defined in Annex C of [22], is the normalized power gain, which could cause inappropriate evaluation of the impact of the antennas as it neglects the fundamental fact that the higher the antenna gain is, the narrower is the beamwidth. However, $G(\phi)$ is acceptable for this work since the authors focus on comparing propagation models, not the antennas. Thus, the definition of $G(\phi)$ can be used here for compatibility purposes with the 3GPP LTE channel model.

$$G(\phi) = -\min\left[12\left(\frac{\phi}{\phi_{3\,\mathrm{dB}}}\right)^2, G_{\mathrm{m}}\right], \quad |\phi| \le 180^\circ. \quad (9)$$

For the EBS, it is assumed that multipaths are confined in the same horizontal plane. Note that the assumption is reasonable for the measurement environment as will be discussed in Section 6.2. For the MS antenna configurations, it is assumed that an elevation power gain, $G(\vartheta)$, has the same expression as in (9). The power gain for the MS antenna configuration is then given as

$$G(\phi,\vartheta) = G(\phi)G(\vartheta), \quad |\phi| \le 180^\circ,\ |\vartheta| \le 90^\circ. \quad (10)$$

It should be noted that all element polarization vectors for the BS and MS are assumed to be unchanged over all directions according to [22].

4.2. Polarimetric Kronecker Product Approximations. In zero-mean complex circularly symmetric Gaussian channels, $\mathbf{H}$ is fully described by its second-order fading statistics, that is, by a full channel correlation matrix, $\mathbf{R}$, which is

$$\mathbf{R} = E[\mathrm{vec}(\mathbf{H})\ \ \mathrm{vec}(\mathbf{H})^H], \quad (11)$$

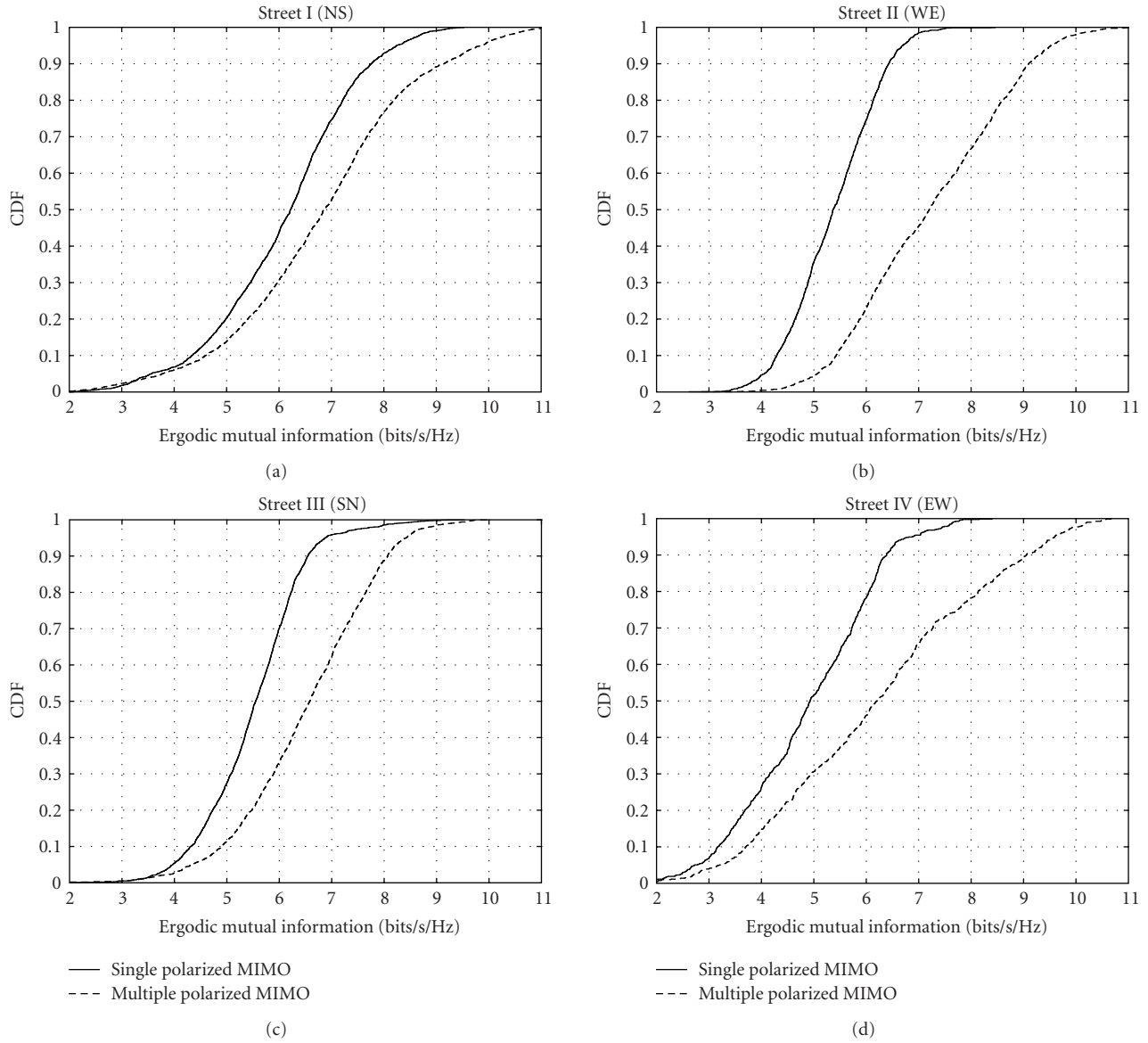

Figure 5: Ergodic mutual information of the single and multiple polarized MIMO systems.

where vec$(\cdot)$ stacks the columns of $\mathbf{H}$ into a column vector, while $E(\cdot)$ and $(\cdot)^H$ are the expectation operator and the Hermitian transpose, respectively.

The conventional Kronecker product approximation [2, 18] models $\mathbf{R}$ by $\mathbf{R}^{\text{Con}}$, which is the Kronecker product of the BS and MS antenna correlation matrices, that is, $\mathbf{R}^{\text{BS}}$ and $\mathbf{R}^{\text{MS}}$, respectively. That is

$$\mathbf{R}^{\text{Con}} = \frac{1}{\text{tr}(\mathbf{R}^{\text{MS}})}\mathbf{R}^{\text{BS}} \otimes \mathbf{R}^{\text{MS}}, \tag{12}$$

where $\otimes$ denotes the Kronecker product,

$$\begin{aligned} \mathbf{R}^{\text{BS}} &= E[\mathbf{H}^T\mathbf{H}^*], \\ \mathbf{R}^{\text{MS}} &= E[\mathbf{H}\mathbf{H}^H]. \end{aligned} \tag{13}$$

$(\cdot)^T$ and $(\cdot)^*$ indicate the transpose and the complex conjugate, respectively. Note that the denominator term, $\text{tr}(\mathbf{R}^{\text{MS}})$, is used to equalize the traces of $\mathbf{R}$ and $\mathbf{R}^{\text{Con}}$.

For single polarization transmission, the conventional Kronecker product approximation was experimentally shown to well predict the ergodic mutual information and ergodic capacity of MIMO systems in [18, 30, 31], in this case, its validity of the performance prediction implies how well the joint angular PSD between the BS and MS can be modeled as the product of the marginal angular PSDs [21].

However, for multiple polarized MIMO systems, the conventional Kronecker product is not suitable to be used for evaluating the separability of the joint angular PSD since the channel polarizations are mixed with the antenna polarizations.

Recently, in the framework of 3GPP LTE, the 3GPP LTE Kronecker product approximation has been proposed to

Table 3: Reference antenna configurations.

Antenna configurations	Value
BS	See Figure 6
Type	2 spatially separated dual polarized antennas
No. of elements	4
Element polarization vectors ($\mathbf{p}$)	$\pm 45^\circ$
Antenna spacing (d_{BS})	4 wavelengths (at 4.5 GHz)
Position vector ($\vec{r}_{n_{\mathrm{BS}}}$)	$-(d_{\mathrm{BS}}/2)\mathbf{u}_y$ for $n_{\mathrm{BS}} = 1, 2$ $(d_{\mathrm{BS}}/2)\mathbf{u}_y$ for $n_{\mathrm{BS}} = 3, 4$
Parameters of $G(\phi)$	$\phi_{3\,\mathrm{dB}} = 70^\circ$, $G_{\mathrm{m}} = 20$ dB
MS: *Laptop* scenario	See Figure 7
Type	2 spatially separated dual polarized antennas
No. of elements	4
Element polarization vectors ($\mathbf{p}$)	$0^\circ, 90^\circ$
Antenna spacing (d_{MS})	2 wavelength (at 4.5 GHz)
Position vector ($\vec{r}_{n_{\mathrm{MS}}}$)	$-(d_{\mathrm{MS}}/2)\mathbf{u}_y$ for $n_{\mathrm{MS}} = 1, 3$ $(d_{\mathrm{MS}}/2)\mathbf{u}_y$ for $n_{\mathrm{MS}} = 2, 4$
Parameters of $G(\phi)$	$\phi_{3\,\mathrm{dB}} = 90^\circ$, $G_{\mathrm{m}} = 10$ dB

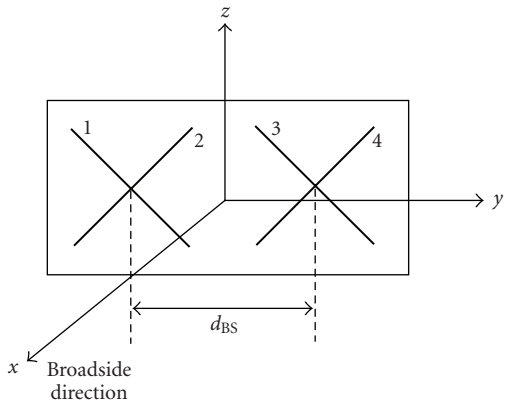

Figure 6: BS antenna configuration [22].

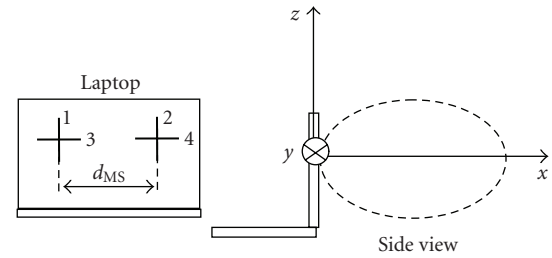

Figure 7: *Laptop* MS antenna configuration [22].

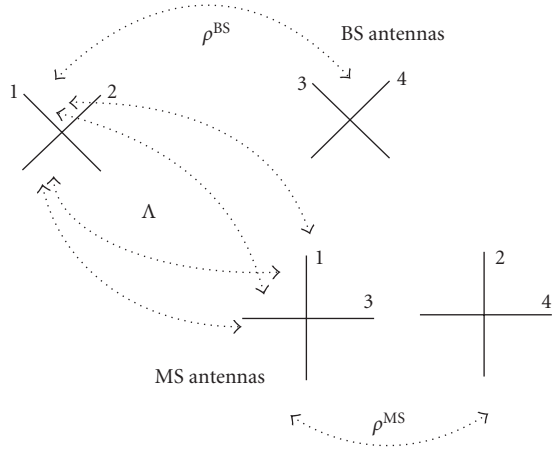

Figure 8: 3GPP LTE Kronecker approximation for the *Laptop* scenario.

model the polarimetric 3GPP LTE channel model [22]. Here, $\mathbf{R}$ is approximated by $\mathbf{R}^{\mathrm{3GPP}}$, which is the Kronecker product of the polarization covariance matrix and the BS and MS spatial correlation matrices as follows:

$$\mathbf{R}^{\mathrm{3GPP}} = \begin{bmatrix} 1 & (\rho^{\mathrm{BS}})^* \\ \rho^{\mathrm{BS}} & 1 \end{bmatrix} \otimes \mathbf{\Lambda} \otimes \begin{bmatrix} 1 & (\rho^{\mathrm{MS}})^* \\ \rho^{\mathrm{MS}} & 1 \end{bmatrix}, \quad (14)$$

where ρ^{BS} and ρ^{MS} are the spatial correlation coefficients between 2 identical omnidirectional antenna elements assumed at the BS and MS, respectively, while $\mathbf{\Lambda}$ is the polarization covariance matrix of the colocated polarization antenna elements, $\mathbf{H}_{\mathrm{pol}}$. It is obtained as follows:

$$\mathbf{\Lambda} = E[\mathrm{vec}(\mathbf{H}_{\mathrm{pol}}) \ \ \mathrm{vec}(\mathbf{H}_{\mathrm{pol}})^H]. \quad (15)$$

In the *Laptop* scenario, $\mathbf{H}_{\mathrm{pol}}$ is vectorized as $[[\mathbf{H}]_{11}, [\mathbf{H}]_{31}, [\mathbf{H}]_{12}, [\mathbf{H}]_{32}]$.

The definitions of ρ^{BS}, ρ^{MS}, and Λ are depicted in Figure 8 for the *Laptop* scenario. Note that (14) is only applicable for the standard antenna configuration of the 3GPP LTE channel model, which was presented in Figure 6.

Interesting work on the polarimetric Kronecker product approximation has been proposed by Shafi et al., in [11]. Based on an analytical derivation by assuming certain PSD models, the use of the sum of channel polarization pair-wise Kronecker products has been proposed to model the full correlation matrix of the 2D SCM model. However, its validity has not been verified or compared with the above mentioned Kronecker product approximations by using real measurement data. Moreover, its extension to 3D case has not been discussed.

By using the similar concept, the authors propose the following general form of the sum of channel polarization pair-wise Kronecker products approximation, which the authors shortly call as the "sum of Kronecker products," to investigate the Kronecker separability of the joint correlation matrix for each channel polarization pair

$$\mathbf{R}^{\mathrm{Sum}} = \sum_{\alpha,\beta=\{\mathrm{V,H}\}} \frac{1}{\mathrm{tr}(\mathbf{R}^{\mathrm{MS}}_{\beta\alpha})} \mathbf{R}^{\mathrm{BS}}_{\beta\alpha} \otimes \mathbf{R}^{\mathrm{MS}}_{\beta\alpha}, \quad (16)$$

where

$$\mathbf{R}_{\beta\alpha}^{\mathrm{BS}} = E[\mathbf{H}_{\beta\alpha}{}^{T}\mathbf{H}_{\beta\alpha}{}^{*}],$$
$$\mathbf{R}_{\beta\alpha}^{\mathrm{MS}} = E[\mathbf{H}_{\beta\alpha}\mathbf{H}_{\beta\alpha}{}^{H}]. \tag{17}$$

$\mathbf{H}_{\beta\alpha}$ is a single polarization MIMO channel matrix for a $\beta\alpha$ polarization pair defined in (3).

The MIMO channel matrix by using the Kronecker product approximations, $\mathbf{H}^{\mathrm{Kron}}$, can be obtained as

$$\mathrm{vec}(\mathbf{H}^{\mathrm{Kron}}) = \hat{\mathbf{R}}^{1/2}\mathrm{vec}(\mathbf{A}), \tag{18}$$

where $\hat{\mathbf{R}}$ is the approximated full correlation matrix. It is replaced by either $\mathbf{R}^{\mathrm{Con}}$, $\mathbf{R}^{\mathrm{3GPP}}$, or $\mathbf{R}^{\mathrm{Sum}}$ in the equation above. $\mathbf{A}$ is an i.i.d. random fading matrix with zero-mean and unity-variance, circularly symmetric complex Gaussian entries. Note that in general once a correlation matrix is given, whether or not it is the Kronecker model, and all entries of the correlation matrix are according to the correlated Rayleigh fading, (18) is always applicable.

5. Evaluation Criterion, Process, and Results

When extending the angular-delay PSD channel model in [20] to the double-directional PSD channel model, it is necessary to know the error of the assumption that the joint correlation matrix can be separated for each polarization pair. By using the proposed sum of Kronecker products, the error is investigated in this section.

5.1. Criterion. The ergodic mutual information introduced in Section 3.3 is used as a criterion to evaluate the Kronecker product approximations. The ergodic mutual information of the Kronecker product approximations, $\mathcal{I}^{\mathrm{Kron}}(n_a)$, can be obtained by replacing the normalized $\mathbf{H}(n_a)$ with the normalized $\mathbf{H}^{\mathrm{Kron}}(n_a)$ in (7). $\mathbf{H}^{\mathrm{Kron}}(n_a)$ is an MIMO channel matrix by applying the Kronecker product approximations to the full correlation matrix of $\mathbf{H}(n_a)$.

However, it should be noted that the normalizations of both measurement and Kronecker product approximations-based instantaneous MIMO channel matrices in this section are done with respect to an MS configuration considered as shown in the following equation for the measurement-based instantaneous MIMO channel matrix, $\tilde{\mathbf{H}}^{(n_r,n_f)}(n_a)$:

$$\tilde{\mathbf{H}}^{(n_r,n_f)}(n_a) = \frac{\mathbf{H}^{(n_r,n_f)}(n_a)}{\sqrt{(1/N_rN_fN_aN_{\mathrm{BS}}N_{\mathrm{MS}})\sum_{n_r=1}^{N_r}\sum_{n_a=1}^{N_a}\sum_{n_f=1}^{N_f}\left\|\mathbf{H}^{(n_r,n_f)}(n_a)\right\|_F^2}}. \tag{19}$$

The absolute percentage of the prediction error is calculated as

$$\varepsilon_{\mathcal{I}^{\mathrm{Kron}}}(n_a) = \frac{\left|\mathcal{I}^{\mathrm{Kron}}(n_a) - \mathcal{I}(n_a)\right|}{\mathcal{I}(n_a)} \times 100\,[\%]. \tag{20}$$

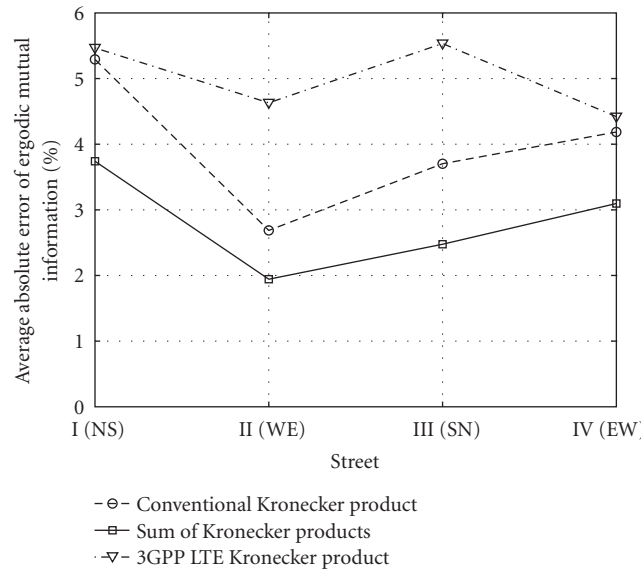

Figure 9: Average absolute errors of ergodic mutual information of the *Laptop* scenario.

5.2. Process. This is how the authors proceed with the evaluation.

(1) Synthesize measurement-based random MIMO channel matrices, $\mathbf{H}$, by using the same values of N_r, N_f, and N_a as explained in Section 3.3.

(2) Obtain $\mathbf{R}^{\mathrm{Con}}$, $\mathbf{R}^{\mathrm{3GPP}}$, and $\mathbf{R}^{\mathrm{Sum}}$ by using (12), (14), and (16). The expectations of the correlation matrices in (13), (15), and (17) are substituted into (18) to synthesize the MIMO channel matrix by using the Kronecker product approximations. This is repeated $N_r \times N_f$ times.

(3) Compare criteria calculated from $\mathbf{H}^{\mathrm{Kron}}$ with $\mathbf{H}$.

5.3. Results. In the evaluation, $\mathcal{I}(n_a)$ and $\mathcal{I}^{\mathrm{Kron}}(n_a)$ are calculated at an SNR of 10 dB. As an example, Figure 10 shows $\mathcal{I}(n_a)$ and $\mathcal{I}^{\mathrm{Kron}}(n_a)$ at MS8 of the *Laptop* scenario. The variation of $\mathcal{I}(n_a)$ and $\mathcal{I}^{\mathrm{Kron}}(n_a)$ with the MS antenna orientation can be clearly seen in the figure. Investigating the accuracy of the predicted $\mathcal{I}^{\mathrm{Kron}}(n_a)$ is done by comparing $\mathcal{I}(n_a)$ and $\mathcal{I}^{\mathrm{Kron}}(n_a)$ of the same MS antenna orientation at a measurement snapshot.

Figure 9 shows the average $\varepsilon_{\mathcal{I}^{\mathrm{Kron}}}$ over the MS antenna orientations and the measurement snapshots in a street, as a function of streets of the *Laptop* scenario. As can be seen, the sum of Kronecker products approximation gives the most accurate prediction of the ergodic mutual information as compared to the others for all measurement streets. While the 3GPP LTE Kronecker product approximation seems to be the worst. This performance degradation could be because of the use of the common correlation coefficients for different colocated polarized antenna elements. Among all streets, street II (WE), where multiple scattering occurs due to its only NLOS characteristic, seems to be most suitable street for applying the Kronecker product approximations.

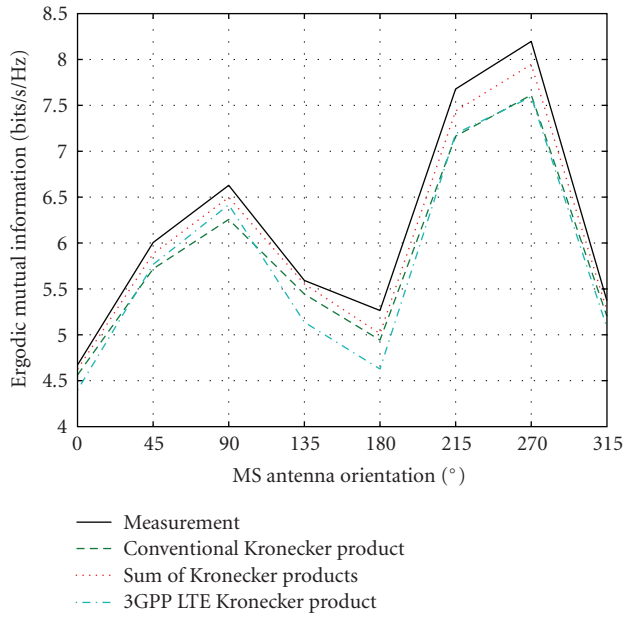

Figure 10: Ergodic mutual information at MS8 of the *Laptop* scenario.

6. Double-Directional Channel Modeling

From the viewpoint of the propagation channel, the validity of the sum of Kronecker product in (16) implies that the joint angular PSD between the BS and MS can be reasonably modeled as the product of the marginal angular PSDs at the BS and MS *when the same single channel polarization-pair is considered*. Mathematically, this can be expressed as

$$P_{\beta\alpha}(\acute{\phi}^{\mathrm{BS}}, \vartheta^{\mathrm{BS}}, \phi^{\mathrm{MS}}, \vartheta^{\mathrm{MS}}) \approx P_{\beta\alpha}(\acute{\phi}^{\mathrm{BS}}, \vartheta^{\mathrm{BS}}) P_{\beta\alpha}(\phi^{\mathrm{MS}}, \vartheta^{\mathrm{MS}}), \tag{21}$$

where $P_{\beta\alpha}(\acute{\phi}^{\mathrm{BS}}, \vartheta^{\mathrm{BS}}, \phi^{\mathrm{MS}}, \vartheta^{\mathrm{MS}})$, $P_{\beta\alpha}(\acute{\phi}^{\mathrm{BS}}, \vartheta^{\mathrm{BS}})$, and $P_{\beta\alpha}(\phi^{\mathrm{MS}}, \vartheta^{\mathrm{MS}})$ are the joint angular PSD, marginal angular PSDs at the BS and MS for a $\{\beta\alpha\}$ polarization-pair, respectively. Note that since measurement snapshots have different ABSs toward the MS, the extracted ABS, ϕ^{BS}, are thus recalculated, so that the ABS of the MS position becomes 0° when obtaining PSDs relating to the ABS. $\acute{\phi}^{\mathrm{BS}}$ denotes the ABS centered at the MS position.

Based on this approximation, the angular-delay PSD channel model at the MS, which has been proposed by the authors in [20], is extended to the double-directional PSD channel model in this paper.

6.1. Angular-Delay PSD Model at MS [20]. In [20], the authors studied the angular-delay channel parameters at the MS in the measurements. The study was carried out for the individual street to clarify the influence of the street direction. By observing the street-based PSDs of AMS (i.e., AMSPSDs), it was clear that they were not ideally uniform. They consist of peak-like components and a residual part, which is the complementary part of the peak-like components. Peak-like components were considered to represent site-specific dominant propagation mechanisms. The peak-like components are identified visually and each is called a class. Table 4 of [20] summarized the identified classes together with their mean EMSs and mean excess delays.

Table 4: Angular-delay PSD model.

Channel parameter	Proposed model
AMSPSD	
$P^{c}_{\beta\alpha}(\phi^{\mathrm{MS}})$	truncated Gaussian PSD
$P^{\mathrm{r}}_{\beta\alpha}(\phi^{\mathrm{MS}})$	uniform PSD
EMSPSD	
$P^{c}_{\beta\alpha}(\vartheta^{\mathrm{MS}})$	general double exponential PSD
$P^{\mathrm{r}}_{\beta\alpha}(\vartheta^{\mathrm{MS}})$	general double exponential PSD
EDPSD	
$P^{c}_{\beta\alpha}(\acute{\tau})$	general double exponential PSD
$P^{\mathrm{r}}_{\beta\alpha}(\acute{\tau})$	general double exponential PSD
Power variation	
$\Gamma^{c}_{\beta\alpha}$	correlated log-normal distribution
$\Gamma^{\mathrm{r}}_{\beta\alpha}$	correlated log-normal distribution

By using their AMSs, mean EMSs, and mean excess delays, the identified classes were connected to the street directions to show their site-specific propagation mechanisms. Table 5 of [20] showed the classification result according the following categorization: *BS-direction*, *street-direction*, *opposite BS-direction*, and *rooftop-diffraction*. The definition of each categorization was described in detail in [20, Section 5].

For the classes and the residual part, the angular-delay PSD channel models were next presented as a product of marginal channel parameter PSDs.

A class or the residual part is considered to exist if its power is larger than zero. While the residual part always exists due to its large occupied AMS, a class can possibly disappear at some measurement snapshots. To take the travel of the MS into account, when a class or the residual part exists, its polarization dependent power variation was modeled by the lognormal distribution with the correlation coefficient matrices between the power values of different polarization pairs of the same multipath component.

In summary, the angular-delay PSD channel model for a $\{\beta\alpha\}$ polarization pair was proposed as

$$P_{\beta\alpha}(\phi^{\mathrm{MS}}, \vartheta^{\mathrm{MS}}, \acute{\tau}) = \sum_{c=1}^{N_c} \Gamma^{c}_{\beta\alpha} P^{c}_{\beta\alpha}(\phi^{\mathrm{MS}}) P^{c}_{\beta\alpha}(\vartheta^{\mathrm{MS}}) P^{c}_{\beta\alpha}(\acute{\tau}) + \Gamma^{\mathrm{r}}_{\beta\alpha} P^{\mathrm{r}}_{\beta\alpha}(\phi^{\mathrm{MS}}) P^{\mathrm{r}}_{\beta\alpha}(\vartheta^{\mathrm{MS}}) P^{\mathrm{r}}_{\beta\alpha}(\acute{\tau}), \tag{22}$$

where $P^{c,\mathrm{r}}_{\beta\alpha}(\phi^{\mathrm{MS}})$, $P^{c,\mathrm{r}}_{\beta\alpha}(\vartheta^{\mathrm{MS}})$, and $P^{c,\mathrm{r}}_{\beta\alpha}(\acute{\tau})$ are the AMSPSD, PSD of EMS (i.e., EMSPSD), and PSD of excess delay (i.e., EDPSD) for a $\{\beta\alpha\}$ polarization pair of the cth class or the

Table 5: Simulation conditions.

Parameters		Value
Number of frequency bins (N_f)		25 in a BW of 120 MHz
Number of antenna azimuth orientations (N_a)		8 with a step of 45°
Number of simulated power variation (N_s)		200
Number of simulated random phase (N_r)		200
Path generation of ABS		
Path number		5
Path spacing		2°
Path generation of AMS		
Path number	of a class	4
	of a residual part	16–21 (varies with streets)
Path spacing	for classes	3°–5° (varies with classes)
	for residual parts	14°
Path generation of EMS		
Path number	of a class	18
	of a residual part	18
Path spacing	for classes	10°
	for residual parts	10°
Path generation of excess delay		
Path number	of a class	80
	of a residual part	80
Path spacing	for classes	8 ns
	for residual parts	8 ns
Path power		Follow a corresponding marginal PSD
Path correlation		0 (independently random path phase)

Table 6: Absolute errors of ergodic mutual information.

	CDF [%]		
Street	10	50	90
I (NS)	10.7	1.7	0.5
II (WE)	4.0	5.1	9.7
III (SN)	4.4	7.0	6.9
IV (EW)	11.3	3.1	2.3

residual part, respectively. The excess delay, $\acute{\tau}$, was obtained as $\acute{\tau} = \tau - \tau_0$, where τ_0 denotes the delay of the first arriving multipath at a measurement snapshot.

$\Gamma_{\beta\alpha}^{c,\mathrm{r}}$ is the power variation of the cth class or the residual part and N_c is the number of classes. All PSDs are normalized to unity. The marginal PSD models are briefly summarized in Table 4. Their best-fit parameters, which were obtained from fitting the PSD models and their corresponding measured PSDs, were listed in the tables in the appendix of [20].

However, since LOS paths traveling through the west side streets were included in the *BS-direction* classes, that is, the 4th class of street I (NS) and the 2nd of street III (SN), the best-fit parameters of the *BS-direction* classes obtained in NLOS environments only are presented in Table 7.

6.2. Angular PSDs at BS. The measured PSD of $\acute{\phi}^{\mathrm{BS}}$, that is, ABSPSD, is found to be well described by the truncated Laplacian PSD [32]. For a $\{\beta\alpha\}$ polarization pair, the truncated Laplacian PSD, $P_{\beta\alpha}(\acute{\phi}^{\mathrm{BS}})$, is expressed as follows:

$$P_{\beta\alpha}(\acute{\phi}^{\mathrm{BS}}) \propto \exp\left[-\frac{\sqrt{2}\,|\acute{\phi}^{\mathrm{BS}} - \acute{\phi}_{0,\beta\alpha}^{\mathrm{BS}}|}{\sigma_{\acute{\phi}_{\beta\alpha}^{\mathrm{BS}}}} \right], \tag{23}$$

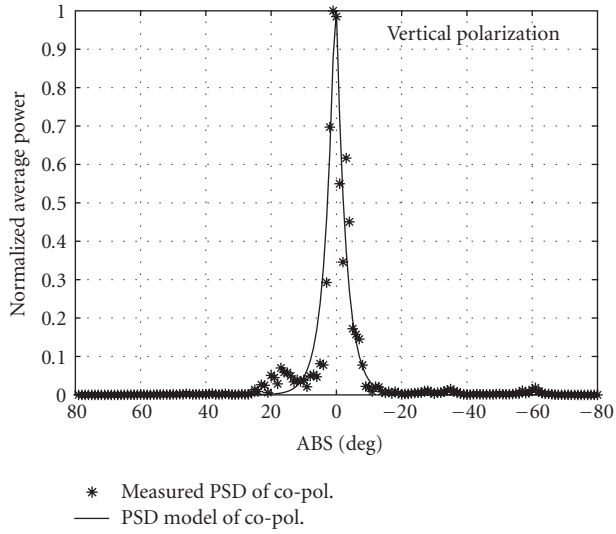

Figure 11: ABSPSDs for a {VV} of street I (NS). 0° is the ABS towards the MS.

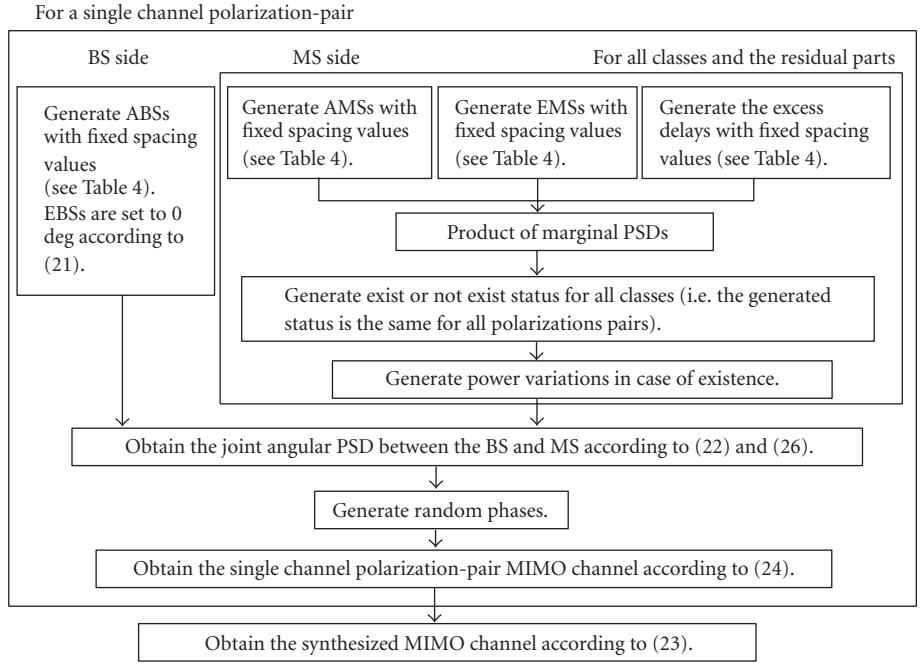

Figure 12: Simulation procedure.

Table 7: Best-fit parameters of *BS-direction* classes for NLOS environments.

		$P^c_{\beta\alpha}(\phi^{\mathrm{MS}})$ VV/HV/HH/VH		
Street	Class no.	$\phi^{c,\mathrm{MS}}_{0,\beta\alpha}$ [°]	$\sigma_{\phi^{c,\mathrm{MS}}_{\beta\alpha}}$ [°]	
I (NS)	4	–102.6/ −104.8/ −103.0/ −92.0	9.2/13.5/9.3/32.5	
III (SN)	2	69.7/69.8/68.9/83.1	11.6/26.3/9.5/36.5	
		$P^c_{\beta\alpha}(\vartheta^{\mathrm{MS}})$ VV/HV/HH/VH		
Street	Class no.	$\vartheta^{c,\mathrm{MS}}_{0,\beta\alpha}$ [°]	$\sigma^{+}_{\vartheta^{c,\mathrm{MS}}_{\beta\alpha}}$ [°]	$\sigma^{-}_{\vartheta^{c,\mathrm{MS}}_{\beta\alpha}}$ [°]
I (NS)	4	10.4/8.0/10.7/13.5	9.8/25.3/10.0/30.4	4.9/3.7/4.6/10.0
III (SN)	2	7.0/7.0/7.0/18.0	8.8/18.7/8.1/16.8	5.6/3.9/5.1/16.0
		$P^c_{\beta\alpha}(\acute{\tau})$ VV/HV/HH/VH		
Street	Class no.	$\acute{\tau}^c_{0,\beta\alpha}$ [ns]	$\sigma^{+}_{\acute{\tau}^c_{\beta\alpha}}$ [ns]	$\sigma^{-}_{\acute{\tau}^c_{\beta\alpha}}$ [ns]
I (NS)	4	4.0/4.0/4.0/4.0	7.6/7.8/7.9/8.8	–/ – / – /–
III (SN)	2	4.8/5.6/4.6/5.6	7.5/5.8/8.1/5.7	–/ – / – /–
		$f(\check{\Gamma}^c_{\beta\alpha})$ VV/HV/HH/VH		
Street	Class no.	Life time	$\check{\Gamma}^{c,\mathrm{r}}_{0,\beta\alpha}$ [dB]	$\sigma_{\Gamma^{c,\mathrm{r}}_{\beta\alpha}}$ [dB]
I (NS)	4	0.98	–116.8/ −127.3/ −116.7/ −128.6	9.9/9.2/10.2/9.0
III(SN)	2	0.96	–117.6/ −128.6/ −117.9/ −129.4	10.4/8.3/9.9/8.3

where $\acute{\phi}^{\mathrm{BS}}_{0,\beta\alpha}$ and $\sigma_{\acute{\phi}^{\mathrm{BS}}_{\beta\alpha}}$ are the mean ABS and spread parameter, respectively. Their best-fit parameters are obtained from fitting $P_{\beta\alpha}(\acute{\phi}^{\mathrm{BS}})$ and the measured ABSPSD, which is calculated by summing the power of a $\{\beta\alpha\}$ polarization pair within a 1° angular bin. Figure 11 shows the measured and modeled ABSPSDs of a {VV} polarization pair of street I (NS). Interestingly, the main peak of the measured ABSPSD is very close to 0° even though the measurements are in NLOS environments. This implies that most multipaths between the BS and MS travel over the rooftop of surrounding buildings around the MS. Table 8 lists the best-fit parameters of the ABSPSD model.

As to the PSD of EBS, for example, EBSPSD, the EBSPSD is confined to its peak of between −9° and −7° depending on streets. The EBSPSD is thus assumed to be a delta function for simplicity, that is,

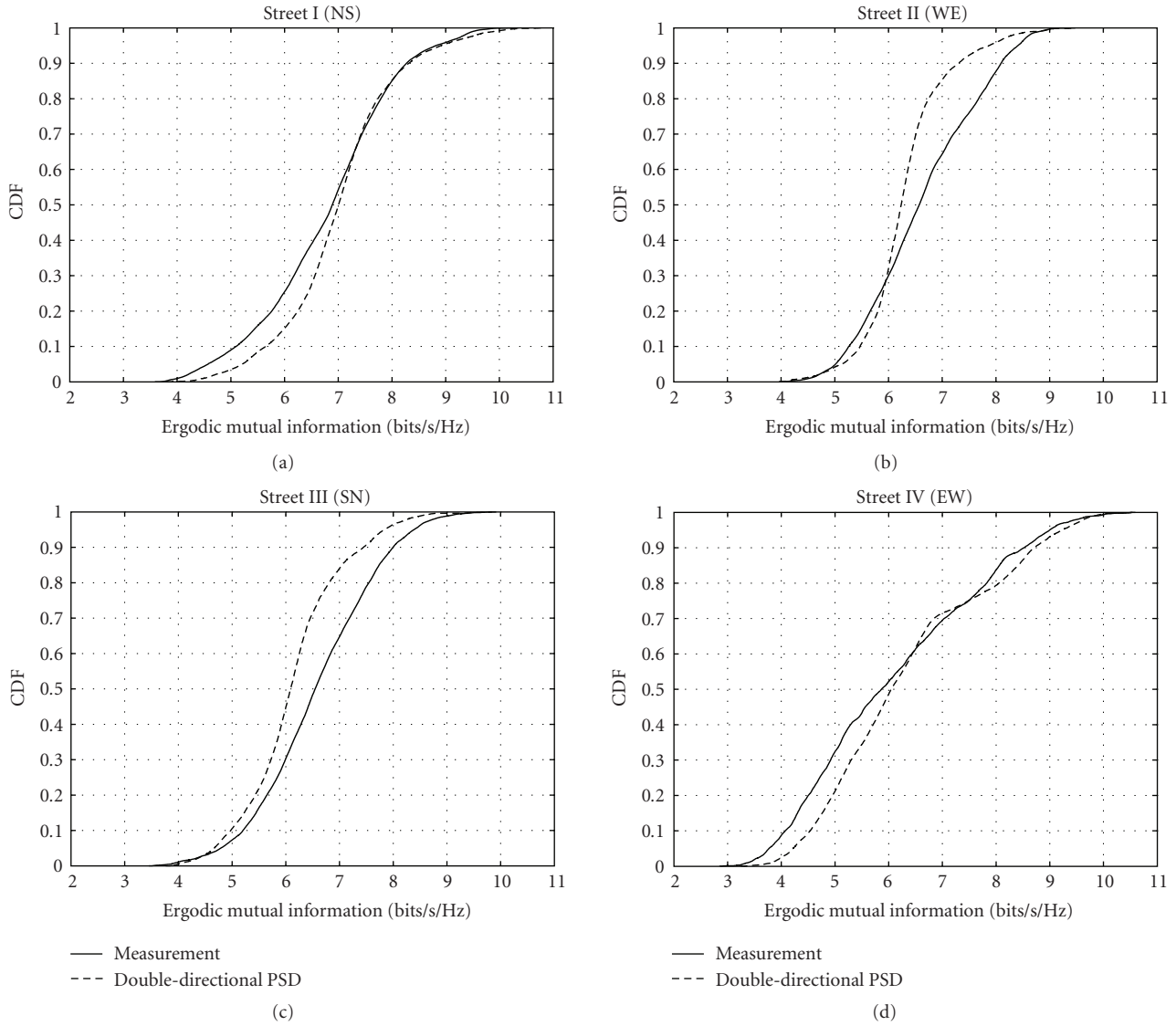

Figure 13: Measured and modeled ergodic mutual information for the *Laptop* scenario.

Table 8: Best-fit parameters of $P_{\beta\alpha}(\acute{\phi}^{\mathrm{BS}})$.

	VV/HV/HH/VH	
Street	$\acute{\phi}^{\mathrm{BS}}_{0,\beta\alpha}$ [°]	$\sigma_{\acute{\phi}^{\mathrm{BS}}_{\beta\alpha}}$ [°]
I (NS)	0.3/0.7/0.7/0.9	4.3/4.9/3.0/2.2
II (WE)	0.4/0.5/0.5/0.6	1.8/1.5/1.8/1.3
III (SN)	1.5/1.4/1.6/1.5	1.7/1.5/1.2/1.1
IV (EW)	1.5/2.5/2.3/1.7	2.5/2.3/2.6/2.0

$$P_{\beta\alpha}(\vartheta^{\mathrm{BS}}) = \delta(\vartheta^{\mathrm{BS}}). \tag{24}$$

In other words, multipaths are assumed to be incident to the horizontal plane. The BS antenna pattern, whose response varies only in the ABS direction, is thus reasonable for the measured environment.

Using (21)–(24), the double-directional PSD for a $\{\beta\alpha\}$ polarization pair is proposed as

$$\begin{aligned} &P_{\beta\alpha}(\acute{\phi}^{\mathrm{BS}}, \vartheta^{\mathrm{BS}}, \phi^{\mathrm{MS}}, \vartheta^{\mathrm{MS}}, \acute{\tau}) \\ &\quad = P_{\beta\alpha}(\acute{\phi}^{\mathrm{BS}}) P_{\beta\alpha}(\vartheta^{\mathrm{BS}}) P_{\beta\alpha}(\phi^{\mathrm{MS}}, \vartheta^{\mathrm{MS}}, \acute{\tau}). \end{aligned} \tag{25}$$

7. Model Evaluation

To evaluate the double-directional PSD channel model, the ergodic mutual information is used. The ergodic mutual information from the synthesized MIMO channel by using the proposed double-directional PSD channel model, that is, $\mathbf{H}^{\mathrm{Model}}(f)$, is compared with the results from the directly synthesized MIMO channel matrix, $\mathbf{H}(f)$. In the model evaluation, the same reference scenario as in the evaluation of the Kronecker separability is assumed.

$\mathbf{H}^{\text{Model}}(f)$ is obtained by using the following equations:

$$\left[\mathbf{H}^{\text{Model}}(f)\right]_{n_{\text{MS}}n_{\text{BS}}} = \sum_{\alpha,\beta=\{\text{V,H}\}} \left[\mathbf{H}^{\text{Model}}_{\beta\alpha}(f)\right]_{n_{\text{MS}}n_{\text{BS}}}, \tag{26}$$

where $\left[\mathbf{H}^{\text{Model}}_{\beta\alpha}(f)\right]_{n_{\text{MS}}n_{\text{BS}}}$ denotes the $(n_{\text{MS}}, n_{\text{BS}})$ element of single polarization $\mathbf{H}^{\text{Model}}(f)$ of a $\{\beta\alpha\}$ polarization pair, that is,

$$\begin{aligned}\left[\mathbf{H}^{\text{Model}}_{\beta\alpha}(f)\right]_{n_{\text{MS}}n_{\text{BS}}} = \sum_{k=1}^{K} \gamma^{\text{Model}}_{\beta\alpha,k} g_{\beta}^{n_{\text{MS}}}(\phi_k^{\text{MS}}, \vartheta_k^{\text{MS}}) g_{\alpha}^{n_{\text{BS}}}(\phi_k^{\text{BS}}, \vartheta_k^{\text{BS}}) \\ \times \exp\left(j\left[\langle \mathbf{k}_k^{\text{MS}}(f), \vec{r}_{n_{\text{MS}}}\rangle + \langle \mathbf{k}_k^{\text{BS}}(f), \vec{r}_{n_{\text{BS}}}\rangle\right]\right. \\ \left. - j2\pi f \tau_k + j\nu_k^{\beta\alpha}\right),\end{aligned} \tag{27}$$

$$\gamma^{\text{Model}}_{\beta\alpha,k} = \sqrt{P_{\beta\alpha}(\phi_k^{\text{BS}}, \vartheta_k^{\text{BS}}, \phi_k^{\text{MS}}, \vartheta_k^{\text{MS}}, \tau_k)}. \tag{28}$$

Multipaths at the BS and MS are generated independently as suggested by (25). That is

$$\gamma^{\text{Model}}_{\beta\alpha,k} = \sqrt{P_{\beta\alpha}(\phi^{\text{BS}})P_{\beta\alpha}(\vartheta^{\text{BS}})P_{\beta\alpha}(\phi^{\text{MS}}, \vartheta^{\text{MS}}, \tau)}. \tag{29}$$

7.1. Simulation Procedure. Figure 12 shows the simulation procedure diagram of multipaths at the BS and MS. All simulation conditions are summarized in Table 5.

For the BS, 5 paths with equal ABS spacing are assigned, so that the magnitude of paths approximately follows the truncated Laplacian PSD of ABSPSD. The EBSs of all multipaths are set to 0° according to (24).

For the MS, multipaths are generated according to the simulation procedures described in [20, Section 7.2].

The generation of multipaths for the MS is briefly summarized as follows.

(1) Generate multipaths for the classes and the residual part. The numbers of multipaths and spacings of the AMS, EMS, and excess delay are set according to the values given in Table 5.

(2) For N_s simulations, generate "exist" or "not exist" status of each class. In general, two-state Markov model is used to generate the status [33]. For the residual part, its status is always set to "exist."

(3) In case of existence, generate power variations, $\Gamma^{c}_{\beta\alpha}$ and $\Gamma^{r}_{\beta\alpha}$.

(4) For a realization of power variation, N_a combinations of antenna array orientation are considered as the evaluation of the Kronecker separability.

After generating multipaths at the BS and MS, the N_r simulations of random phases of polarizations between 0 to 2π are next generated, in order to calculate $\mathbf{H}^{\text{Model}}(f)$ according to (26)–(29). As explained in Section 3.1, $\mathbf{H}^{\text{Model}}(f)$ is simply expressed as $\mathbf{H}^{\text{Model}}$.

For the n_ath MS antenna orientation, the ergodic mutual information of $\mathbf{H}^{\text{Model}}$, $\mathcal{I}^{\text{Model}}(n_a)$, can be obtained by replacing the normalized $\mathbf{H}(n_a)$ with the normalized $\mathbf{H}^{\text{Model}}(n_a)$ in (7). $\mathbf{H}^{\text{Model}}(n_a)$ is a $\mathbf{H}^{\text{Model}}$ when the MS antenna orientation is $\phi^{\text{MS}}(n_a)$. It is obtained by replacing ϕ_k^{MS} with $\{\phi_k^{\text{MS}} - \phi^{\text{MS}}(n_a)\}$ in (27), where $\phi^{\text{MS}}(n_a) = 0^\circ, 45^\circ, \ldots, 315^\circ$ for $n_a = 1, \ldots, 8$, respectively. Similar to the evaluation of the Kronecker separability, all ergodic mutual information are calculated at an SNR of 10 dB.

7.2. Results. Figure 13 shows the CDFs of the measured and modeled ergodic mutual information of all frequencies, antenna array orientations, and power variations for the *Laptop* scenario. In general, there is a close agreement between the measured and modeled results. Table 6 summarizes the absolute percentage errors of modeled results from measured results at 10%, 50%, and 90% CDFs. According to the table, the difference was found to be within around 11%, 7%, and 10% at 10%, 50%, and 90% CDFs, respectively.

8. Conclusion

The improvement in the ergodic mutual information of a multiple polarized MIMO system was first verified. Then, the Kronecker separability of the joint polarimetric angular PSD between the BS and MS of the measured propagation channel was investigated by using the ergodic mutual information. The authors showed that the joint polarimetric angular PSD could be modeled as the product of the marginal angular PSDs at the BS and MS when the same single channel polarization pair is considered. From this result, the extension of the angular-delay PSD model proposed previously by the authors to the double-directional PSD channel model was done. The double-directional PSD channel model was verified by comparing the CDFs of the measured and modeled ergodic mutual information. The results were found to be in a good agreement with those obtained from the measurement.

Acknowledgment

This research is supported by the National Institute of Information and Communications Technology of Japan.

References

[1] E. Telatar, "Capacity of multi-antenna Gaussian channels," *European Transactions on Telecommunications*, vol. 10, no. 6, pp. 585–595, 1999.

[2] D.-S. Shiu, G. J. Foschini, M. J. Gans, and J. M. Kahn, "Fading correlation and its effect on the capacity of multielement antenna systems," *IEEE Transactions on Communications*, vol. 48, no. 3, pp. 502–513, 2000.

[3] T. Svantesson and J. Wallace, "On signal strength and multipath richness in multi-input multi-output systems," in *Proceedings of IEEE International Conference on Communications (ICC '03)*, vol. 4, pp. 2683–2687, Anchorage, Alaska, USA, May 2003.

[4] J. B. Andersen and B. N. Getu, "The MIMO cube—a compact MIMO antenna," in *Proceedings of the 5th International Symposium on Wireless Personal Multimedia Communications*

(WPMC '02), vol. 1, pp. 112–114, Honolulu, Hawaii, USA, October 2002.

[5] C.-Y. Chiu, J.-B. Yan, and R. D. Murch, "24-port and 36-port antenna cubes suitable for MIMO wireless communications," *IEEE Transactions on Antennas and Propagation*, vol. 56, no. 4, pp. 1170–1176, 2008.

[6] T. Wirth, V. Jungnickel, A. Forck, et al., "Polarisation dependent MIMO gains on multiuser downlink OFDMA with a 3GPP LTE air interface in typical urban outdoor scenarios," in *Proceedings of the International ITG Workshop on Smart Antennas (WSA '08)*, pp. 157–161, Darmstadt, Germany, February 2008.

[7] L. Dong, H. Choo, R. W. Heath Jr., and H. Ling, "Simulation of MIMO channel capacity with antenna polarization diversity," *IEEE Transactions on Wireless Communications*, vol. 4, no. 4, pp. 1869–1873, 2005.

[8] G. Calcev, D. Chizhik, B. Goransson, et al., "A wideband spatial channel model for system-wide simulations," *IEEE Transactions on Vehicular Technology*, vol. 56, no. 2, pp. 389–403, 2007.

[9] "Spatial channel model for MIMO simulations," Tech. Rep. TR 25.996 V6.1.0, 3GPP, Valbonne, France, September 2003.

[10] L. M. Correia, Ed., *Mobile Broadband Multimedia Networks: Techniques, Models and Tools for 4G*, Academic Press, New York, NY, USA, 2006.

[11] M. Shafi, M. Zhang, A. L. Moustakas, et al., "Polarized MIMO channels in 3-D: models, measurements and mutual information," *IEEE Journal on Selected Areas in Communications*, vol. 24, no. 3, pp. 514–527, 2006.

[12] C. Waldschmidt, C. Kuhnert, T. Fugen, and W. Wiesbeck, "Measurements and simulations of compact MIMO-systems based on polarization diversity," in *Proceedings of IEEE Topical Conference on Wireless Communication Technology (WCT '03)*, pp. 284–285, Honolulu, Hawaii, USA, October 2003.

[13] V. Erceg, P. Soma, D. S. Baum, and S. Catreux, "Multiple-input multiple-output fixed wireless radio channel measurements and modeling using dual-polarized antennas at 2.5 GHz," *IEEE Transactions on Wireless Communications*, vol. 3, no. 6, pp. 2288–2298, 2004.

[14] M. Landmann, K. Sivasondhivat, J.-I. Takada, I. Ida, and R. Thomä, "Polarization behavior of discrete multipath and diffuse scattering in urban environments at 4.5 GHz," *EURASIP Journal on Wireless Communications and Networking*, vol. 2007, Article ID 57980, 16 pages, 2007.

[15] J. Ling, D. Chizhik, D. Samardzija, and R. A. Valenzuela, "Peer-to-peer MIMO radio channel measurements in a rural area," *IEEE Transactions on Wireless Communications*, vol. 6, no. 9, pp. 3229–3237, 2007.

[16] M. Steinbauer, A. F. Molisch, and E. Bonek, "The double-directional radio channel," *IEEE Antennas and Propagation Magazine*, vol. 43, no. 4, pp. 51–63, 2001.

[17] K. Kalliola, H. Laitinen, P. Vainikainen, M. Toeltsch, J. Laurila, and E. Bonek, "3-D double-directional radio channel characterization for urban macrocellular applications," *IEEE Transactions on Antennas and Propagation*, vol. 51, no. 11, pp. 3122–3133, 2003.

[18] J. P. Kermoal, L. Schumacher, K. I. Pedersen, P. E. Mogensen, and F. Frederiksen, "A stochastic MIMO radio channel model with experimental validation," *IEEE Journal on Selected Areas in Communications*, vol. 20, no. 6, pp. 1211–1226, 2002.

[19] W. Weichselberger, M. Herdin, H. Ozcelik, and E. Bonek, "A stochastic MIMO channel model with joint correlation of both link ends," *IEEE Transactions on Wireless Communications*, vol. 5, no. 1, pp. 90–100, 2006.

[20] K. Sivasondhivat, J.-I. Takada, I. Ida, and Y. Oishi, "Experimental analysis and site-specific modeling of channel parameters at mobile station in an urban macrocellular environment," *IEICE Transactions on Communications*, vol. E91-B, no. 4, pp. 1132–1144, 2008.

[21] M. Bengtsson and P. Zetterberg, "Some notes on the Kronecker model," submitted to *EURASIP Journal on Wireless Communications and Networking*.

[22] "LTE channel models and simulations," Tech. Rep. R4-060334, 3GPP, Valbonne, France, February 2006.

[23] R. Thomä, M. Landmann, and A. Richter, "RIMAX—a maximum likelihood framework for parameter estimation in multidimensional channel sounding," in *Proceedings of the International Symposium on Antennas and Propagation (ISAP '04)*, pp. 53–56, Sendai, Japan, August 2004.

[24] A. Ludwig, "The definition of cross polarization," *IEEE Transactions on Antennas and Propagation*, vol. 21, no. 1, pp. 116–119, 1973.

[25] A. F. Molisch, M. Steinbauer, M. Toeltsch, E. Bonek, and R. Thomä, "Capacity of MIMO systems based on measured wireless channels," *IEEE Journal on Selected Areas in Communications*, vol. 20, no. 3, pp. 561–569, 2002.

[26] S. Takahashi and Y. Yamada, "Propagation-loss prediction using ray tracing with a randomphase technique," *IEICE Transactions on Fundamentals of Electronics, Communications and Computer Sciences*, vol. E81-A, no. 7, pp. 1445–1451, 1998.

[27] K. Kalliola, K. Sulonen, H. Laitinen, O. Kivekäs, J. Krogerus, and P. Vainikainen, "Angular power distribution and mean effective gain of mobile antenna in different propagation environments," *IEEE Transactions on Vehicular Technology*, vol. 51, no. 5, pp. 823–838, 2002.

[28] R. G. Vaughan, "Polarization diversity in mobile communications," *IEEE Transactions on Vehicular Technology*, vol. 39, no. 3, pp. 177–186, 1990.

[29] K. Sivasondhivat, *Analysis and modeling of double-directional polarized channel in urban macrocellular environment*, Ph.D. dissertation, Tokyo Institute of Technology, Tokyo, Japan, 2008.

[30] K. Sivasondhivat, J.-I. Takada, Y. Nakaya, I. Ida, and Y. Oishi, "Verification of kronecker MIMO channel model in a NLOS macrocellular environment," in *Proceedings of the IEICE General Conference*, p. 233, Tokyo, Japan, March 2006, B-1-233.

[31] D. P. McNamara, M. A. Beach, and P. N. Fletcher, "Spatial correlation in indoor MIMO channels," in *Proceedings of the 13th IEEE International Symposium on Personal, Indoor and Mobile Radio Communications (PIMRC '02)*, vol. 1, pp. 290–294, Lisbon, Portugal, September 2002.

[32] K. I. Pedersen, P. E. Mogensen, and B. H. Fleury, "Power azimuth spectrum in outdoor environments," *Electronics Letters*, vol. 33, no. 18, pp. 1583–1584, 1997.

[33] C.-C. Chong, C.-M. Tan, D. I. Laurenson, S. McLaughlin, M. A. Beach, and A. R. Nix, "A novel wideband dynamic directional indoor channel model based on a Markov process," *IEEE Transactions on Wireless Communications*, vol. 4, no. 4, pp. 1539–1552, 2005.